Temporal reshaping of two-dimensional pulses

Colin J. R. Sheppard,[1,*] Shan Shan Kou,[2] Jiao Lin,[2] Manjula Sharma[3] and George Barbastathis[4]

[1]*Istituto Italiano di Tecnologia, via Morego 30, Genova 16163, Italy*
[2]*School of Physics, University of Melbourne, Parkville, VIC 3010, Australia*
[3]*School of Physics, University of Sydney, NSW 2006, Australia*
[4]*Department of Mechanical Engineering Massachusetts Institute of Technology 77 Massachusetts Avenue, Cambridge, MA 02139, USA*
colinjrsheppard@gmail.com

Abstract: An analytic study of complete cylindrical focusing of pulses in two dimensions is presented, and compared with the analogous three-dimensional case of focusing over a complete sphere. Such behavior is relevant for understanding the limiting performance of ultrafast, planar photonic and plasmonic devices. A particular spectral distribution is assumed that contains finite energy. Separate ingoing and outgoing pulsed waves are considered, along with the combination that would be generated in free space by an ingoing wave. It is shown that for the two dimensional case, in order to produce a temporally symmetrical pulse at the focus, an asymmetric pulse must be launched. A symmetrical outgoing pulse is generated from a source with asymmetric time behavior, or an anti-symmetric input pulse. These results are very different from the corresponding three-dimensional case, and imply fundamental limitations on the performance of ultrafast, tightly focused, two-dimensional devices.

OCIS codes: (320.5550) Pulses; (260.1960) Diffraction theory.

References and links

1. T. Tyc, "Gouy phase for full-aperture spherical and cylindrical waves," Opt. Lett. **37**(5), 924–926 (2012).
2. J. Lin, J. Dellinger, P. Genevet, B. Cluzel, F. de Fornel, and F. Capasso, "Cosine-Gauss plasmon beam: A localized long-range nondiffracting surface wave," Phys. Rev. Lett. **109**(9), 093904 (2012).
3. P. M. Morse and H. Feshbach, *Methods of Theoretical Physics* (McGraw Hill, New York, 1978).
4. S. Quabis, R. Dorn, M. Eberler, O. Glockl, and G. Leuchs, "Focusing light to a tighter spot," Opt. Commun. **179**(1-6), 1–7 (2000).
5. Y. G. Ma, S. Sahebdivan, C. K. Ong, T. Tyc, and U. Leonhardt, "Evidence for subwavelength imaging with positive refraction," New J. Phys. **13**(3), 033016 (2011).
6. X. Zhang, "Perfect lenses in focus: No drain, no gain," Nature **480**, 42–43 (2011).
7. J. C. Gonzalez, P. Benitez, and J. C. Miñano, "Perfect drain for the Maxwell fish eye lens," New J. Phys. **13**(2), 023038 (2011).
8. A. Sentenac, P. C. Chaumet, and G. Leuchs, "Total absorption of light by a nanoparticle: an electromagnetic sink in the optical regime," Opt. Lett. **38**(6), 818–820 (2013).
9. I. P. Christov, "Propagation of femtosecond light pulses," Opt. Commun. **53**(6), 364–366 (1985).
10. E. Heyman and L. B. Felson, "Complex-source pulsed-beam fields," J. Opt. Soc. Am. A **6**(6), 806–817 (1989).
11. R. W. Ziolkowski, "Localized transmission of electromagnetic energy," Phys. Rev. A **39**(4), 2005–2033 (1989).
12. R. W. Ziolkowski and J. B. Judkins, "Propagation characteristics of ultrawide-bandwidth pulsed Gaussian beams," J. Opt. Soc. Am. A **9**(11), 2021–2030 (1992).
13. J. Y. Lu and J. F. Greenleaf, "Nondiffracting X waves-exact solutions to free-space scalar wave equation and their finite aperture realizations," IEEE Trans. Ultrason. Ferroelectr. Freq. Control **39**(1), 19–31 (1992).
14. E. Heyman and T. Melamed, "Certain considerations in aperture synthesis of ultrawideband/short-pulse radiation," IEEE Trans. Antenn. Propag. **42**(4), 518–525 (1994).
15. A. M. Shaarawi, I. M. Besieris, and R. W. Ziolkowski, "The propagating and evanescent field components of localized wave solutions," Opt. Commun. **116**(1-3), 183–192 (1995).
16. M. M. Wefers and K. A. Nelson, "Space-time profiles of shaped ultrafast optical waveforms," IEEE J. Quantum Electron. **32**(1), 161–172 (1996).
17. C. J. R. Sheppard and X. Gan, "Free-space propagation of femto-second light pulses," Opt. Commun. **133**(1-6), 1–6 (1997).
18. Z. Wang, Z. Zhang, Z. Xu, and Q. Lin, "Space-time profiles of an ultrashort pulsed Gaussian beam," IEEE J. Quantum Electron. **33**(4), 566–573 (1997).

#225555 - $15.00 USD Received 28 Oct 2014; revised 30 Nov 2014; accepted 30 Nov 2014; published 18 Dec 2014

19. D. You and P. H. Bucksbaum, "Propagation of half-cycle far infrared pulses," J. Opt. Soc. Am. B **14**(7), 1651–1655 (1997).
20. S. Feng, H. G. Winful, and R. W. Hellwarth, "Gouy shift and temporal reshaping of focused single-cycle electromagnetic pulses," Opt. Lett. **23**(5), 385–387 (1998).
21. A. E. Kaplan, "Diffraction-induced transformation of near-cycle and sub-cycle pulses," J. Opt. Soc. Am. B **15**(3), 951–956 (1998).
22. G. P. Agrawal, "Spectrum-induced changes in diffraction of pulsed optical beams," Opt. Commun. **157**(1-6), 52–56 (1998).
23. M. A. Porras, "Ultrashort pulsed Gaussian light beams," Phys. Rev. E Stat. Phys. Plasmas Fluids Relat. Interdiscip. Topics **58**(1), 1086–1093 (1998).
24. S. Feng, H. G. Winful, and R. W. Hellwarth, "Spatiotemporal evolution of focused single-cycle electromagnetic pulses," Phys. Rev. E Stat. Phys. Plasmas Fluids Relat. Interdiscip. Topics **59**(4), 4630–4649 (1999).
25. C. F. R. Caron and R. M. Potvliege, "Free-space propagation of ultra-short pulses: space-time couplings in Gaussian pulse beams," J. Mod. Opt. **46**(13), 1881–1891 (1999).
26. S. Feng and H. G. Winful, "Spatiotemporal structure of isodiffracting ultrashort electromagnetic pulses," Phys. Rev. E Stat. Phys. Plasmas Fluids Relat. Interdiscip. Topics **61**(1), 862–873 (2000).
27. P. Saari, "Evolution of subcycle pulses in nonparaxial Gaussian beams," Opt. Express **8**(11), 590–598 (2001).
28. C. J. R. Sheppard and H. J. Matthews, "Imaging in high aperture optical systems," J. Opt. Soc. Am. A **4**(8), 1354–1360 (1987).
29. S. Hell and E. H. K. Stelzer, "Fundamental improvement of resolution with a 4Pi-confocal fluorescence microscope using two-photon excitation," Opt. Commun. **93**(5-6), 277–282 (1992).
30. L. G. Gouy, "Sur une propriété nouvelle des ondes lumineuses," Comptes Rendus de l'Académie des Sciences, Paris **110**, 1251–1253 (1890).
31. I. S. Gradstein and I. M. Ryshik, *Tables of Series, Products, and Integrals* (Harri Deutsch, Thun, 1981).
32. I. M. Gel'fand and G. E. Shilov, *Generalized Functions* (Academic, San Diego, 1964).

1. Introduction

There is currently considerable interest in development of compact, ultrafast devices, based on planar waveguide and plasmonic technology. Recently Tyc discussed how pulses in two dimensions (2D) behave very differently from those in 3D [1], and this effect is critically important in determining the fundamental limitations in performance of such devices. In the frequency domain, 2D behaves in a qualitatively similar fashion to 3D. Different forms of waves in 3D have their analog in 2D, so that, for example, the analog of the Bessel beam is the cosine beam [2]. But in the time domain, 2D and 3D are different. This has actually been known for many years. For example, Morse and Feshbach describe how, in 2D, propagation of a pulse is accompanied by a wake [3]. This behavior of 2D pulses imposes a limit on the combination of high bandwidth and tight focusing.

As the duration of ultra-short laser pulses continues to decrease, it has become necessary to re-examine models for pulsed light beams. These models are also of relevance in terahertz technology. Tyc's model is computational and appreciation of the consequences difficult, and so to explore the behavior further we investigate analytically simple complete spherical or cylindrical scalar pulses in 3D or 2D, respectively. The extension to the electromagnetic case can be performed using the principles of the Hertz potentials. We consider pulsed sources, pulsed sinks, and focused pulses corresponding to sink/source combinations [4–8].

Such pulsed beams can be regarded as a coherent superposition of monochromatic beams with a spectrum of different frequencies. This fact follows directly from the linearity of the Helmholtz equation or Maxwell's equations. We assume a spectral distribution that has finite energy. Note that it is only comparatively recently that the ultrafast community has appreciated the diffraction effects known as space-time couplings, which become important in tight focusing of ultrashort pulses [9–27]. We assume a Gamma spectral distribution [11, 13]

$$\begin{aligned} f(k)\mathrm{d}k &= \frac{1}{k_1}\exp\left(-\frac{k}{k_1}\right)\mathrm{d}k, k > 0 \\ &= 0, k < 0, \end{aligned} \tag{1}$$

where $k = 2\pi/\lambda = \omega/c$ and k_1 is a positive parameter that determines the bandwidth. This spectral distribution is a good model for single-cycle pulses, avoiding the infinite energy of a constant spectrum, and also avoiding the negative frequencies, and possible resulting artifacts,

#225555 - $15.00 USD Received 28 Oct 2014; revised 30 Nov 2014; accepted 30 Nov 2014; published 18 Dec 2014

of a shifted Gaussian distribution when used to describe the transform of an analytic signal [17]. The distribution can be extended to the Pearson Type III distribution, which incorporates a power factor k^s and a shift along the frequency axis. As the power s increases, the distribution then tends towards a shifted Gaussian. These modifications can be incorporated retrospectively in the time domain by making use of the differentiation and shift theorems of Fourier transforms.

2. The 3D case

We start by reviewing pulses in 3D, so that we can compare 2D pulses with them. In spherical polar co-ordinates for the 3D case, we can sum over monochromatic outgoing spherical waves to give

$$\begin{aligned} U(r,t) &= A\int_0^\infty f(k)\frac{\exp(ikr)}{r}\exp(-ikct)\,\mathrm{d}k \\ &= \frac{A}{r}\frac{1}{\left[1+ik_1c\left(t-\frac{r}{c}\right)\right]}, \end{aligned} \tag{2}$$

where A is a constant that has the dimensions of distance. This simple expression represents an outgoing spherical pulse, from a physical radiating point source. Note that the field therefore diverges when $r \to 0$.

If a pulse converges on a point, as for example might be the case in laser fusion experiments, it subsequently diverges so that it can be modeled as a combination of a source and a sink [15], here normalized to unity at $r = 0, t = 0$, to give

$$\begin{aligned} U(r,t) &= \frac{1}{2ik_1r}\left\{\frac{1}{\left[1+ik_1c\left(t-\frac{r}{c}\right)\right]}-\frac{1}{\left[1+ik_1c\left(t+\frac{r}{c}\right)\right]}\right\} \\ &= \frac{1}{k_1^2r^2+(1+ik_1ct)^2}. \end{aligned} \tag{3}$$

This model is also relevant for pulsed 4Pi focusing in microscopy [28, 29]. There is no physical source at the focus and no singularity. This wave does not satisfy Sommerfeld's radiation condition, and does not need to as there must be additional sources present outside of the focal region that generate the ingoing field. At the focus the amplitude is then

$$U(0,t) = \frac{1}{\left(1+ik_1ct\right)^2}, \tag{4}$$

and at time $t = 0$, the amplitude variation in space is

$$U(r,0) = \frac{1}{1+k_1^2r^2}, \tag{5}$$

and so we see that the spatial and temporal behaviors differ. There is no singularity, and there is a compact pulse in space and time. As the pulse collapses to the origin, the ingoing and outgoing components of the pulse interfere constructively, giving a concentration of energy for t = 0. The pulse then diverges in a reverse time sequence. The behavior of the instantaneous amplitude, given by the real part of the complex field, is shown in Fig. 1(a) as a contour plot as function of spherical radius and time. We could instead plot the instantaneous

#225555 - $15.00 USD Received 28 Oct 2014; revised 30 Nov 2014; accepted 30 Nov 2014; published 18 Dec 2014

intensity, given by the square of the real part of the complex field. Note that the squared magnitude of the complex field, on the other hand, gives the pulse envelope, equivalent to the time-averaged intensity. We see that although the pulse is compact in space and time around $r = 0, t = 0$, the source that is needed to generate the pulse, i.e. for large negative time, has an anti-symmetric structure, so that the instantaneous intensity exhibits a double peak. This is a consequence of the Gouy phase shift through focus [20, 24, 30]. The outgoing pulse also has this anti-symmetric structure. If, on the other hand, we propagate a single-peaked pulse (from large negative time), an anti-symmetric peak is then produced at the focus. This latter solution can be modeled by minus the imaginary part of the complex field, i.e. the real part of the product of the complex field and $\exp(-i\delta)$, with $\delta = -\pi/2$. We can calculate a valid physical field from the complex field by assuming any fixed argument. The amplitude behavior of the 3D source/sink pulse in the near field and far field, for different values of δ, is summarized in Fig. 2.

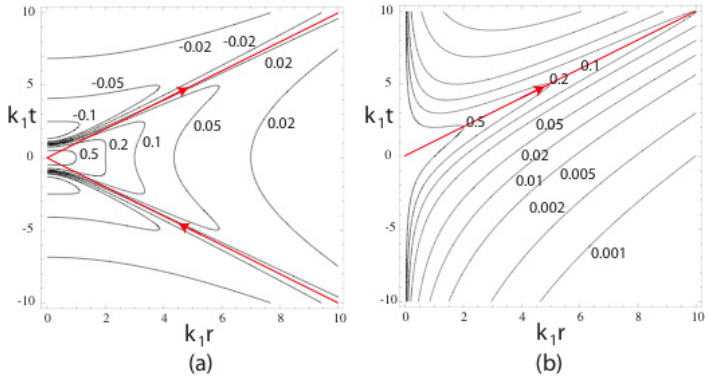

Fig. 1. (a) The real part of the amplitude of a source/sink 3D pulse, given by the instantaneous amplitude for $\delta = 0$, (b) an outgoing 3D pulse, $\delta = -\pi/2$. The light cone is shown in red, with the direction of propagation indicated with arrows.

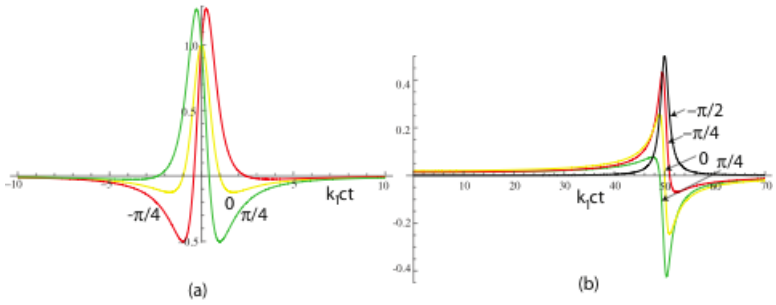

Fig. 2. 3D source/sink pulses for different values of the parameter δ. (a) Amplitude at the focus, normalized to unity at $t = 0$. (b) Output pulse amplitude $(\times k_1 r)$ at $k_1 r = 50$. A symmetrical pulse at the focus produces an antisymmetric output pulse in the far field.

Figures 1(a) and 2 show the behavior if the radiation is not absorbed in the focal region. Absorbing the radiation completely is equivalent to having a sink with no source present. A sink or a source behave similarly to each other, but time-reversed. For the case of a pulsed source in 3D, as given by the source term in Eq. (3), the corresponding plots appear in Fig. 1(b). In order to obtain these results we take $\delta = -\pi/2$. A pulsed source can be generated from a sub-wavelength distribution of currents and charges, as would be the case with an optical antenna. Now at any fixed radius a single-peaked pulse of symmetrical and constant shape in time is detected. At any fixed time, the source term diverges at $r = 0$. The fact that

#225555 - $15.00 USD Received 28 Oct 2014; revised 30 Nov 2014; accepted 30 Nov 2014; published 18 Dec 2014

the pulsed source does not exhibit the Gouy phase effect that the source/sink combination does, suggests that the Gouy phase arises from interference between the source and sink fields, which is consistent with an explanation based on a resonance phenomenon where the sink field gives rise to the source field, as in Huygens' principle. A pulsed sink would behave in a similar fashion to the source, but in reversed time. The effect on the amplitude in the near field and far field of varying δ is shown in Fig. 3, based on the source term in Eq. (3). Taking $\delta = -\pi/2$ gives a symmetrical, compact pulse both at the source and in the far field. Note that at $k_1 r = 50$ the amplitude of the output pulse from the pulsed source is very similar to that of the source/sink. This is because the input pulse in the latter case has decayed to a small value by $k_1 ct = 50$.

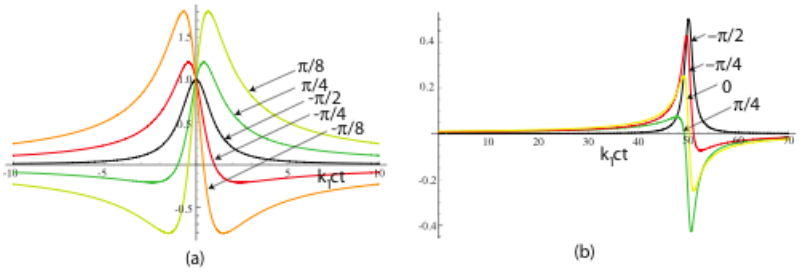

Fig. 3. 3D pulsed source for different values of the parameter δ. (a) Amplitude at the source, normalized to unity at $t = 0$. (b) Output pulse amplitude $(\times k_1 r)$.

3. The 2D Case

Now that we have reviewed the behavior for 3D pulses, we consider pulses in 2D. For an outgoing wave we have [31, Eq. 6.611,6]

$$U(\rho,t) = A\int_0^\infty f(k) H_0^{(1)}(k\rho)\exp(-ikct)\,\mathrm{d}k$$
$$= \frac{A}{\sqrt{k_1^2\rho^2 + (1+ik_1ct)^2}}\left\{1 - \frac{2i}{\pi}\ln\left[\frac{1}{k_1\rho} + \frac{ict}{\rho} + \frac{1}{\rho}\sqrt{\rho^2 + \left(\frac{1}{k_1} + ict\right)^2}\right]\right\}, \quad (6)$$

where ρ is the cylindrical radius, $H_0^{(1)}$ is a Hankel function, and A is a constant; and similarly for an ingoing wave

$$U(\rho,t) = \frac{A}{\sqrt{k_1^2\rho^2 + (1+ik_1ct)^2}}\left\{1 + \frac{2i}{\pi}\ln\left[\frac{1}{k_1\rho} + \frac{ict}{\rho} + \frac{1}{\rho}\sqrt{\rho^2 + \left(\frac{1}{k_1} + ict\right)^2}\right]\right\}. \quad (7)$$

Adding these together ensures that the singularities cancel, and normalizing to unity at the origin for zero time, we obtain for the combined source/sink solution

$$U(\rho,t) = \frac{1}{\sqrt{k_1^2\rho^2 + (1+ik_1ct)^2}}. \quad (8)$$

We can see from Eq. (8) that, unlike the expression for the 3D case in Eq. (3), this expression cannot be split into ingoing and outgoing components using partial fractions. Again we show a contour plot in Fig. 4(a), calculated directly from Eq. (8). In the contour plot of Fig. 4(a), the intensity is greatest outside the light 'cone' defined by $ct = \pm\rho$, i.e. for $\rho > \pm ct$. We note

#225555 - $15.00 USD Received 28 Oct 2014; revised 30 Nov 2014; accepted 30 Nov 2014; published 18 Dec 2014

that for a causal pulse we would expect the intensity to be zero for $\rho > \pm ct$, but our assumed pulse shape is not causal in time. Using the analytic signal representation, ultra-short pulses are modeled as non-causal, and observed experimental pulses are likewise non-causal.

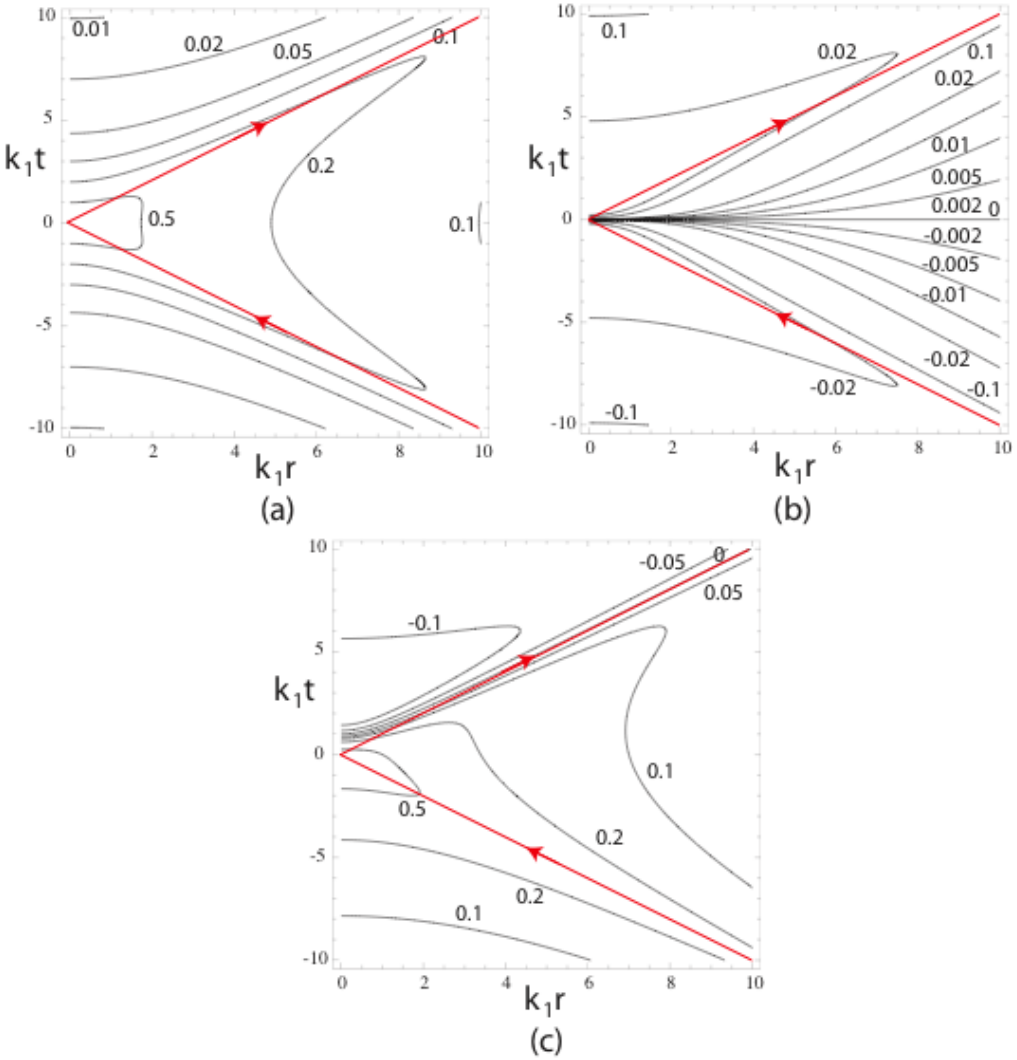

Fig. 4. The amplitude of different 2D source/sink pulses generated by different launched input pulse shapes: (a) launched by an input pulse with a wake, $\delta = 0$, (b) an input pulse with a slow rise, $\delta = -\pi/2$, (c) symmetric input pulse, anti-symmetric output pulse, $\delta = \pi/4$. The light 'cone' is shown in red, with the direction of propagation indicated with arrows.

Although the pulse is compact around $\rho = 0, t = 0$ as for the 3D case (as seen from the 0.5 contour in Fig. 4(a)), the ingoing and outgoing pulses are broad and overlap in time, as seen by comparing Fig. 4(a) (where the amplitude at $t = 0$ falls off slowly with r) with Fig. 1(a). On the other hand, the anti-symmetric pulse structure we saw with 3D does not exist here. This is because the Gouy phase through focus from far field to far field for 2D is $\pi/2$, rather than the π we have for 3D (as was pointed out by Gouy himself [30]). As a function of time or radius, the pulse exhibits an asymmetric shape, as seen from the 0.1 contours in Fig. 4(a) as compared with Fig. 1(a) for the 3D case.

#225555 - $15.00 USD Received 28 Oct 2014; revised 30 Nov 2014; accepted 30 Nov 2014; published 18 Dec 2014

As before, the instantaneous intensity, an observable time-resolved quantity, is given by the square of the real part of the complex field. For the source/sink wave the instantaneous intensity is given by

$$I(\rho,t)=\frac{1+k_1^2(\rho^2-c^2t^2)}{2\left[1+2k_1^2(\rho^2+c^2t^2)+k_1^4(\rho^2-c^2t^2)^2\right]} + \frac{1}{2\sqrt{1+2k_1^2(\rho^2+c^2t^2)+k_1^4(\rho^2-c^2t^2)^2}}. \tag{9}$$

In order to investigate the asymptotic behavior, we now introduce the retarded time

$$t'=t-\rho/c \tag{10}$$

into Eq. (9). Then assuming ρ is large, we obtain far from the focus

$$I(\rho,t')=\frac{1}{4k_1\rho}\left[\frac{1}{\sqrt{1+k_1^2c^2t'^2}}-\frac{k_1ct'}{(1+k_1^2c^2t'^2)}\right]. \tag{11}$$

Equation (11) is a reversed version of the function

$$f(x)=\frac{1}{\sqrt{1+x^2}}+\frac{x}{(1+x^2)}, \tag{12}$$

as shown in Fig. 5(a). The two terms in Eq. (12) are symmetric and antisymmetric, respectively, and tend to cancel for negative x (positive t'). For positive x (negative t') they reinforce to produce a wake. As compared with the symmetric 3D case, in which the instantaneous intensity has a full width at half maximum (FWHM) of $k_1ct=2$, for the 2D case the FWHM is 3.15. This is actually smaller than the FWHM of the square root term alone, which is $2\sqrt{3}=3.46$. But the wake decays only as $2/k_1ct$, so that the full width at one tenth of the maximum is 16.63 (compared with 6.00 for the 3D case).

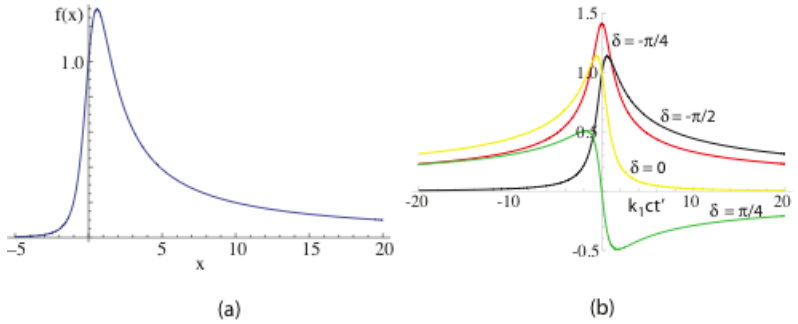

Fig. 5. (a) The function $f(x)$. (b) The instantaneous amplitude in the far field for different values of δ, as given by Eq. (14).

As before, we can calculate a valid physical field from the complex field in Eq. (8) by assuming any fixed argument. For example, assuming that the observed field is given by minus the imaginary part of Eq. (8), i.e. the real part of the product of the complex field and $\exp(-i\delta)$, with $\delta=-\pi/2$, gives rise to an amplitude of the form shown in Fig. 4(b). As compared with Fig. 4(a) we see that, as a result of the antisymmetric behavior near the origin, the intensity is greatest for $\rho<\pm ct$. Figure 4(c) shows the behavior for a phase of $\delta=\pi/4$,

#225555 - $15.00 USD Received 28 Oct 2014; revised 30 Nov 2014; accepted 30 Nov 2014; published 18 Dec 2014

which is seen to correspond to the case when a symmetrical pulse is launched from the far field, giving a distorted pulse near the origin, and an anti-symmetric pulse in the outgoing far field. Then for $\rho = 0$, we see that

$$U(0,t) = \frac{1 - k_1 ct}{1 + (k_1 ct)^2}. \tag{13}$$

Far from the focus, we can write for the time resolved amplitude of the outgoing pulse in the general case

$$U(\rho,t') = \frac{\cos(\delta + \frac{\pi}{4})\left(\sqrt{1 + k_1^2 c^2 t'^2} + 1\right)^{1/2} - \mathrm{sgn}(t')\sin(\delta + \frac{\pi}{4})\left(\sqrt{1 + k_1^2 c^2 t'^2} - 1\right)^{1/2}}{\sqrt{4k_1\rho(1 + k_1^2 c^2 t'^2)}}. \tag{14}$$

The time resolved amplitude is illustrated for different values of δ in Fig. 5(b). The antisymmetric pulse ($\delta = \pi/4$) has a time-resolved intensity with a FWHM of $k_1 ct = 13.51$, and a full width at tenth maximum of $k_1 ct = 77.92$. The symmetric pulse ($\delta = -\pi/4$) has a time-resolved intensity with a FWHM of $k_1 ct = 2.54$, and a full width at tenth maximum of $k_1 ct = 11.54$. Figure 6 shows the time resolved amplitude for the input pulse, in the focal region, and the output pulse, all calculated directly from Eq. (8). The output pulses in Fig. 6(c) agree well with those in Fig. 5(b). A symmetric pulse in the near field gives a far field with a slow rise and sharp fall ($\delta = 0$). This is generated by an input pulse with sharp rise and slow fall, i.e. the closest to a causal pulse. The most symmetrical output pulse is achieved for $\delta = -\pi/4$, and the most symmetrical input pulse is for $\delta = \pi/4$. The best compromise between near field and far field (output) pulse lengths is around $\delta \approx -\pi/8$. Then the intensity FWHM of the output pulse is $k_1 ct = 2.68$ and the full width at tenth maximum is $k_1 ct = 12.72$. The effect of changing δ on the pulse shapes is summarized in Fig. 6 (Media 1), which is a movie showing how the spatial amplitude variation ($\times\sqrt{k_1 r}$ to make the peak amplitude approximately constant) changes with time: an input pulse is launched from the far field (negative time), travels towards $r = 0$ at time $t = 0$, and then gives rise to an output pulse. In particular, a symmetrical input pulse ($\delta = \pi/4$, green curve in Fig. 6 (Media 1)) gives rise to an anti-symmetric output pulse, and vice-versa for the red curve ($\delta = -\pi/4$).

For large $k_1 ct'$, the wake gives an amplitude that falls off with a relationship $h(x)/x^{1/2}$, where $h(x)$ is a Heaviside step function. This has been shown to be equivalent to a fractional order derivative (half order) of a step function, $\sqrt{\pi}h^{(1/2)}(x)$ [32].

For a 2D outgoing pulse, as given in Eq. (6), as could be launched from an optical antenna, we find that a symmetric pulse shape in the near field is given by the imaginary part $\delta = -\pi/2$, whereas the real part, or the $\delta = -\pi/4$ case, give rise to asymmetric pulses in the near field. The resulting behavior for the symmetric case, $\delta = -\pi/2$, is illustrated in Fig. 7. At a fixed distant position the instantaneous amplitude rises suddenly and then drops slowly. There is a logarithmic singularity at $\rho = 0, t = 0$. As $\rho \to 0$, the instantaneous amplitude for the source tends to become symmetrical in time. In the far field the pulse shape becomes identical to the source/sink solution, as plotted in Fig. 5(b).

#225555 - $15.00 USD Received 28 Oct 2014; revised 30 Nov 2014; accepted 30 Nov 2014; published 18 Dec 2014

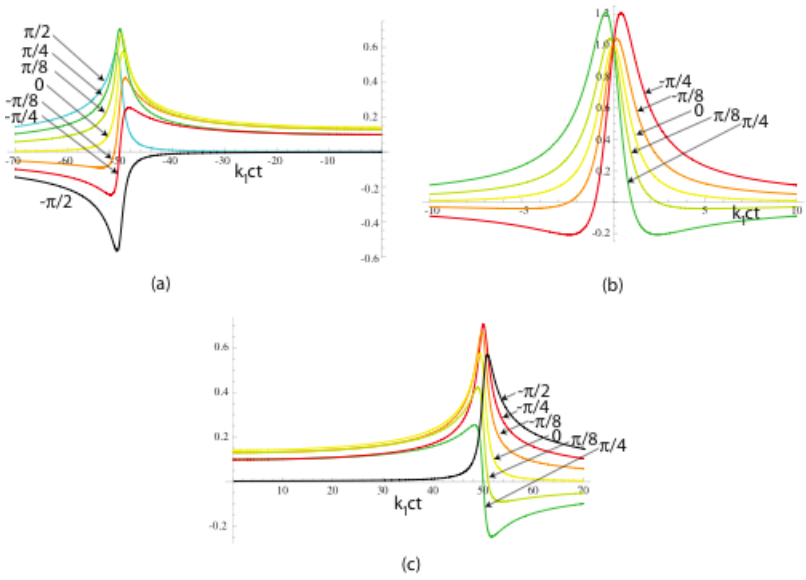

Fig. 6. 2D source/sink pulses for different values of the parameter δ. (a) Time variation of the input pulse amplitude at $k_1 r = 50$, multiplied by $\sqrt{k_1 r} = \sqrt{50}$. (b) Time variation of the amplitude at the source/sink, normalized to unity at $t = 0$. (c) Time variation of the output pulse amplitude at $k_1 r = 50$, multiplied by $\sqrt{k_1 r} = \sqrt{50}$. See Media 1: a movie showing how the amplitude variation $(\times\sqrt{k_1 r})$ in space changes with time.

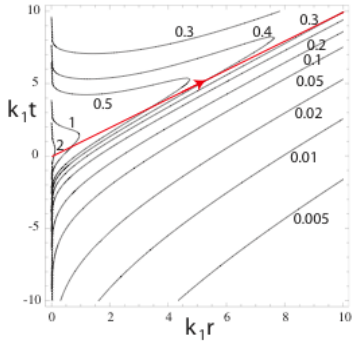

Fig. 7. A 2D outgoing pulse generated by a time-symmetric source, $\delta = -\pi/2$. The light 'cone' is shown in red, with the direction of propagation indicated with an arrow. The output pulse decays slowly above the light 'cone'.

The effect of varying δ on a 2D source is summarized in Fig. 8. The far field is almost the same as the output pulse in Fig. 6. For $\delta = \pm\pi/2$ the near-field pulse is symmetric, but the far-field pulse has a wake (sharp rise and slow fall). For $\delta = -\pi/4$ the output pulse is symmetric, but the near-field pulse has a slow rise, a sign change and then a slow fall. A compromise between near field and far field pulse lengths occurs when $\delta \approx -3\pi/8$, when the far field pulse shape is the time reversal of that for $\delta \approx -\pi/8$ (described above for the source/sink case). Figure 8 (Media 2) is a movie showing how the spatial amplitude variation ($\times\sqrt{k_1 r}$ to make the peak amplitude approximately constant) changes with time: a time-symmetric source ($\delta = \pm\pi/2$, black and turquoise curves, respectively) gives rise to an

#225555 - $15.00 USD Received 28 Oct 2014; revised 30 Nov 2014; accepted 30 Nov 2014; published 18 Dec 2014

output pulse with a wake, whereas in order to produce a symmetric output pulse ($\delta = -\pi/4$, red curve) requires an asymmetric excitation, more easily seen in Fig. 8(a).

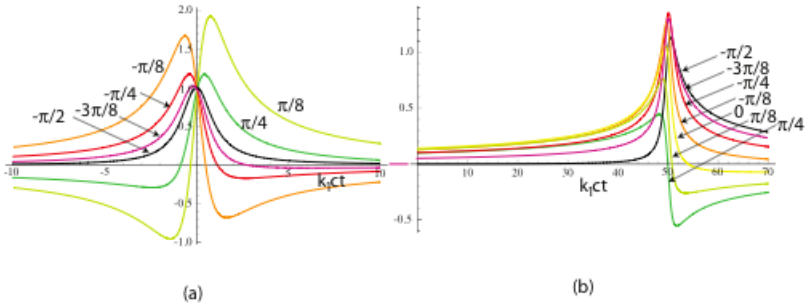

Fig. 8. The amplitude of a 2D pulsed source for different values of the parameter δ . (a) Time variation of the amplitude at the source, normalized to unity at $t = 0$. (b) Time variation of the output pulse amplitude at $k_1 r = 50$, multiplied by $\sqrt{k_1 r} = \sqrt{50}$. See Media 2: a movie showing how the amplitude variation $(\times\sqrt{k_1 r})$ in space changes with time.

4. Discussion

Pulsed beams can be generated by summing over monochromatic beams, with the assumption of a particular spectral distribution. Observable time resolved quantities are the instantaneous field or the instantaneous intensity. The squared magnitude of the complex amplitude, on the other hand, gives the envelope, or time-averaged intensity.

Monochromatic 2D and 3D focusing systems behave in similar ways, but pulsed systems exhibit considerable fundamental differences. As a simple analytic model, we considered complete circular or spherical focusing, in 2D and 3D, respectively. We considered the case of an ingoing wave, which subsequently expands to give an outgoing wave. In 3D, an ingoing, single symmetrical pulse gives rise to an anti-symmetric, double pulse in the focus. In order to achieve a symmetric focal pulse, an anti-symmetric pulse must be launched from the far field. This effect results from the Gouy phase. In 2D, as the total Gouy phase is $\pi/2$ rather than π , the behavior is different. An asymmetric pulse, with a slow rise, must be launched in order to give a symmetrical pulse at the focus. If a symmetric pulse is launched, the focal pulse is asymmetric, and the outgoing pulse is anti-symmetric.

We also considered a pulsed outgoing wave from a source, equivalent to a pulsed, spatial Green function. In 3D the outgoing pulse propagates without change to its temporal shape. In 2D, a symmetrical pulsed source gives rise to an asymmetric pulse in the far field, and vice-versa.

These observations have bearing on the limiting performance of photonic planar devices based on tightly focused ultrashort pulses.

Acknowledgments

C. J. R. Sheppard thanks the University of Melbourne for a Lyle Fellowship. S. S. Kou and J. Lin are recipients of the Discovery Early Career Researcher Award funded by the Australian Research Council under projects DE120102352 and DE130100954, respectively.

#225555 - $15.00 USD Received 28 Oct 2014; revised 30 Nov 2014; accepted 30 Nov 2014; published 18 Dec 2014